

WFC3 Instrument Science Report 2008-28

WFC3 IR Ground P-Flats

H. Bushouse
December 23, 2008

ABSTRACT

IR external flat field exposures from WFC3 thermal-vacuum campaign 3 have been used to construct and deliver an initial set of IR pixel-to-pixel flat field reference files for the 15 imaging filters in the WFC3 IR channel. The flats have a mean signal-to-noise ratio of ~500, which yields corrections down to a level of ~0.2%. The flats have some artifacts related to their ground-based origin, which will need to be addressed in order to properly calibrate on-orbit images. These data show that the IR4 flight detector easily meets and exceeds the applicable IR flat field-related CEI requirements.

Introduction

We have created an initial set of IR pixel-to-pixel flat field (PFL) reference images for the WFC3 IR-4 flight detector from the calibration data obtained in the third and final thermal vacuum campaign (TV3) at Goddard Space Flight Center in February-April 2008. The reference files have been delivered to the Calibration Database System (CDBS), where they are available for use in calibration pipeline processing.

Data

The TV3 flat field exposures were obtained using two versions of the IR13S01 ground-test Science Mission Specification (SMS): IR13S01A and IR13S01B. This SMS obtains one flat field exposure in each of the 15 IR channel imaging filters, using the WFC3 external optical stimulus (OS) as the illumination source. The OS tungsten lamp was used with the monochromator set to “mirror” mode, which produced a continuous spectrum over the entire wavelength range of the IR channel for all of the filters. All exposures

used the SPARS10 sample sequence for the readout mode, with varying numbers of readouts (samples) per exposure. The number of readouts was chosen to obtain a signal of $\sim 60,000$ e^-/pix in the final read. The “B” version of the SMS used a reduced number of reads for a few exposures that went into saturation in the “A” version. The SMS was run a total of 4 times throughout TV3 (once for the “A” version and three times for the “B” version), yielding a total of 4 exposures for combining into a reference flat for each filter. Two runs were performed when WFC3 was operating on MEB1 and the other two on MEB2. A detailed list of the images is given in Appendix A.

Note that flat-fielding of grism observations is accomplished using a data cube of monochromatic flats. The acquisition and processing of ground-test data for these reference files is described in a separate report by Kuntschner et al. (2008).

Data Processing

The individual exposures were processed and combined into reference files using the Python scripts described in Bushouse (2008). The scripts are a modified version of those used to create the WFC3 UVIS bias, dark, and flat-field reference files (Martel et al. 2008; Sabbi 2008). The scripts use the standard WFC3 calibration program `calwf3` to first calibrate each individual exposure and then use the IRAF task `imcombine` to combine the exposures for a given filter into a final flat field image.

Before processing, the reference file keywords in the headers of the raw FITS files were updated to use the most recent IR bad pixel table (BPIXTAB), detector parameters table (CCDTAB), dark file (DARKFILE), and non-linearity correction file (NLINFILE). The specific reference files that were used are recorded in the headers of the flat-field files delivered to CDBS. The calibration steps applied by `calwf3` included data quality initialization (DQICORR), zeroth read signal correction (ZSIGCORR), reference pixel bias correction (BLEVCORR), zeroth read subtraction (ZOFFCORR), dark subtraction (DARKCORR), and non-linearity correction (NLINCORR).

The `calwf3` IR up-the-ramp fitting and cosmic-ray rejection step (CRCORR) has not yet been completely optimized for WFC3 IR data, so rather than using ramp fits to compute the final value for each pixel we chose to simply use the data from an individual readout in the IMA file produced by `calwf3` as the final calibrated image for each exposure. The final readout was used for most exposures. For the 4 overexposed sequences obtained with the IR13S01A SMS we used the second-to-last readout, which gave signals that were below the saturation level. The Python scripts allow the user to specify which readout of each IMA file to use as input to `imcombine`.

The calibrated images were combined using `imcombine` with the `reject` parameter set to “`ccdclip`” in order to reject pixels contaminated by cosmic-ray (CR) hits or any other anomalies. The SCI array in the combined image for each filter was normalized to a value of 1.0 over the image section [101:900,101:900], which excludes areas of the detector

known to contain anomalies, such as the “Death Star” and the “Wagon Wheel” (see the next section for a description of these features). The ERR array in the combined images was normalized using the same scale factor as for the SCI array. The DQ arrays have been reset to zero so that when these flats are used to calibrate other science images using `calwf3` the bad pixel flags will come exclusively from the BPIXTAB.

The resulting flat-field reference files were delivered to CDBS and are available in the on-line CDBS WFC3 reference file area “iref” and can also be retrieved from the HST data archive. A list of the reference files is given in Table 1. An image of each of the 15 flats is shown in Appendix B.

Table 1. IR Flat Field Reference Files in CDBS

Reference File Name	IR Filter
sca2025ti_pfl.fits	F098M
sca20260i_pfl.fits	F105W
sca20261i_pfl.fits	F110W
sca20262i_pfl.fits	F125W
sca20263i_pfl.fits	F126N
sca20264i_pfl.fits	F127M
sca20265i_pfl.fits	F128N
sca20266i_pfl.fits	F130N
sca20267i_pfl.fits	F132N
sca20268i_pfl.fits	F139M
sca20269i_pfl.fits	F140W
sca2026ai_pfl.fits	F153M
sca2026bi_pfl.fits	F160W
sca2026ci_pfl.fits	F164N
sca2026di_pfl.fits	F167N

Results

Each individual exposure contained 50,000-60,000 e^-/pix , so that the combined flats have a total of 200,000 to 240,000 e^-/pix . For purely Poisson statistics we expect a noise level of $\sim 0.2\%$ in the combined flats, which is exactly what `imcombine` found for the variation in input pixel values and is subsequently reflected in the ERR arrays of the flats. Application of a combined flat to one of the individual exposures for that filter yields RMS residuals across the image of $\sim 0.5\%$, which is the limit of what is expected for an image with an original signal level of $\sim 55,000 e^-/\text{pix}$.

Figure 1 shows the F140W flat field image, which demonstrates that the quantum efficiency (QE) of the IR4 flight detector is relatively constant over a large fraction of the field. There is, however, a family of QE features that are unique to this detector. First, there are vertical and diagonal lines of pixels scattered across the field that have 5-15% lower QE than the mean. Second, there are several large scale, usually irregularly shaped,

areas of lower than normal (or zero) QE. Some of these have come to be known by familiar names (see Figure 1): the “Death Star” is a circular region of unresponsive pixels near the bottom edge of the detector that has a diameter of ~45 pixels; the “Wagon Wheel” is a large arc-shaped feature in the lower-right corner of the array, getting its name from its distinctive rim and spoke-like shape. The QE of pixels within the Wagon Wheel is typically 25-35% below normal and reaches a minimum of ~50%. Two elongated features to the left and upper left of the Wagon Wheel have QE ~2% higher and ~8% lower than average, respectively. Finally, there are small clumps of unbonded pixels in the upper left and right corners, as well as near the center of the top edge of the detector. These pixels have no response.

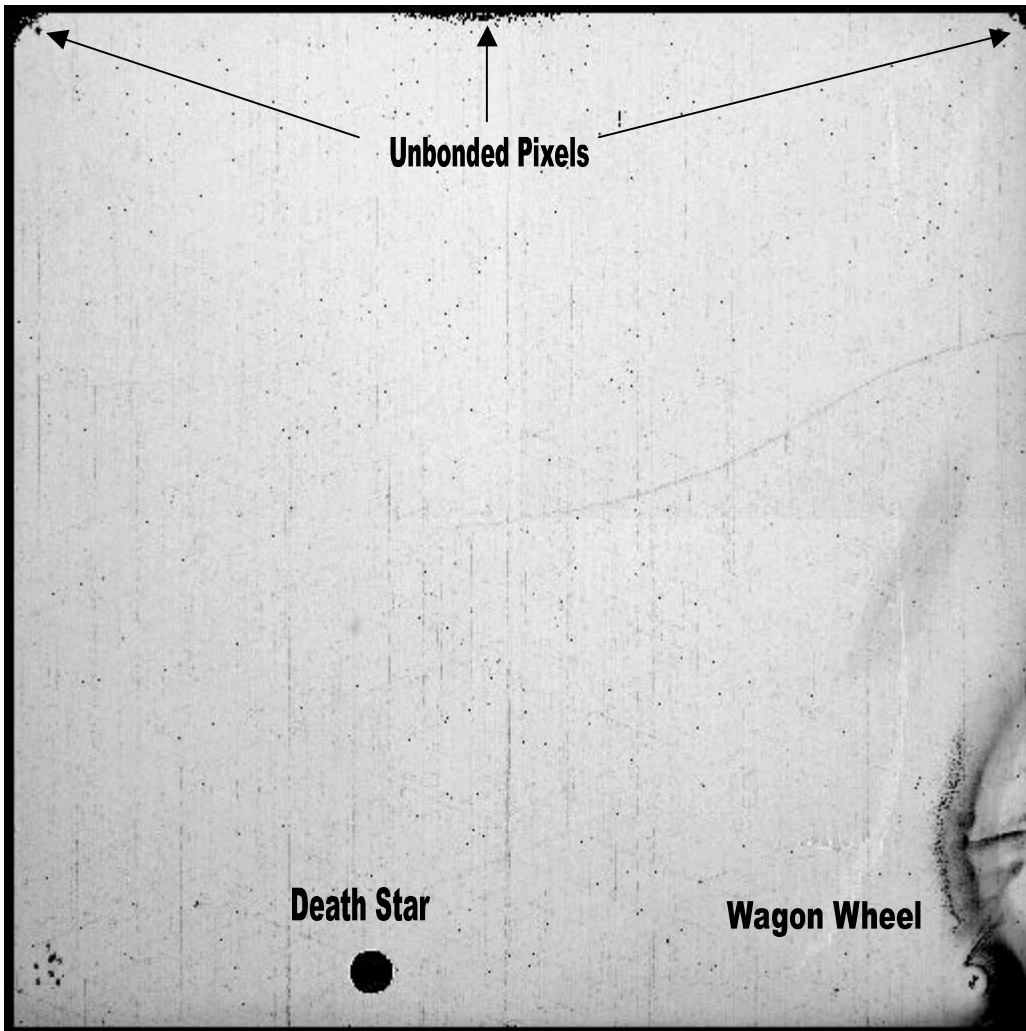


Figure 1. F140W flat field image shown with a positive stretch and familiar labels for some of the prominent features.

The ratio of two individual flat field images for the F110W filter is shown in Figure 2. The ratio image is quite featureless except for the Death Star and the unbonded pixels

at the top corners and edge of the array. This shows that the other low-QE features are very stable and calibrate out very well. The RMS residual in the ratio image is $\sim 0.5\%$.



Figure 2. The ratio of two F110W flat field images.

The large-scale, low QE features show some wavelength dependence. A careful look at the images in Appendix B shows that the Wagon Wheel feature, for example, appears deeper in the short-wavelength filters. This is confirmed in the ratios of flats for the different filters. Figure 3 shows the ratio of the F098M flat to the F167N flat, which spans the entire wavelength range of the IR channel. The vertical and diagonal lines of pixels, as well as the large-scale features like the Wagon Wheel, are lower than average in the ratio, indicating lower QE at shorter wavelengths. The Wagon Wheel area, in particular, is 10-15% lower at short wavelengths, while the remaining features in the ratio image are $\sim 5\%$ low.

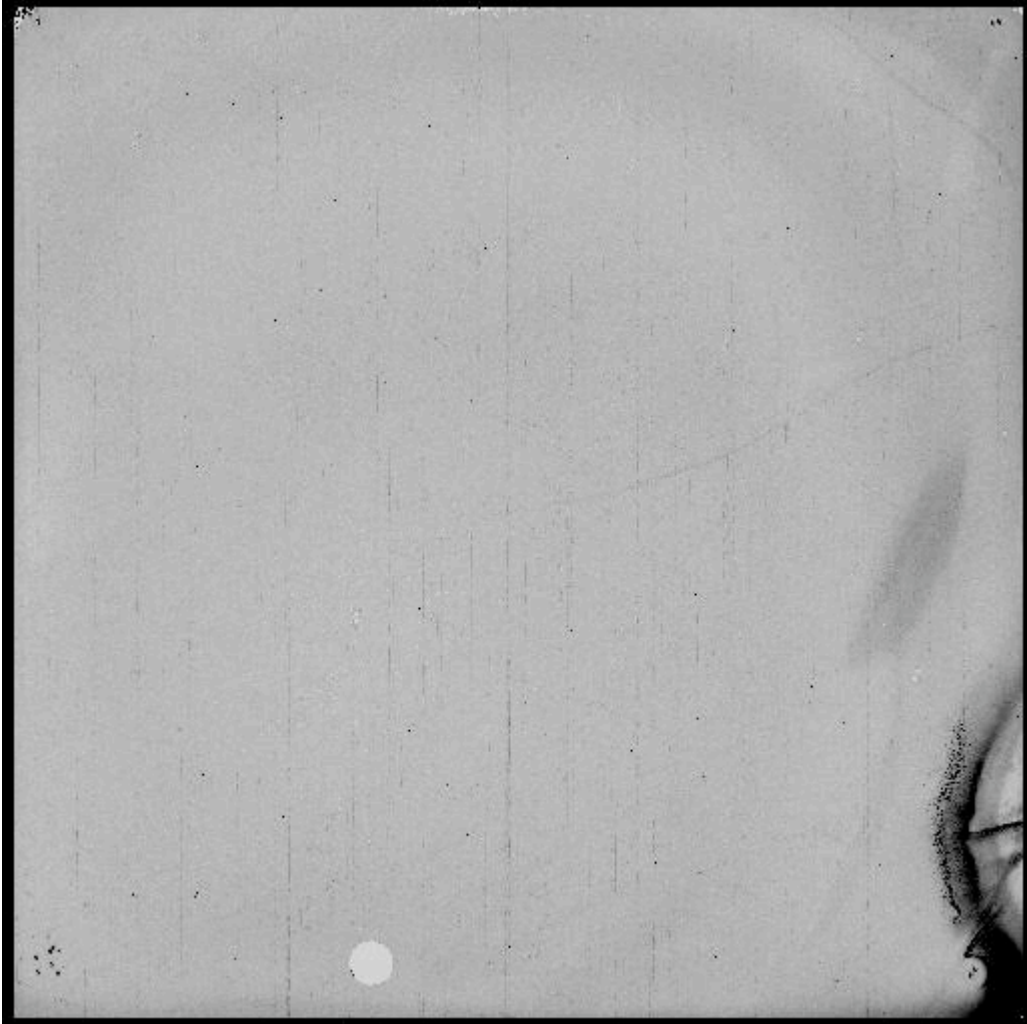


Figure 3. Ratio of the F098M flat to the F167N flat.

The ratios of individual images to the combined flats, as well as the ratios of various individual flat field exposures to one another, show some residual artifacts. Figure 4 shows an example, which is the ratio of the F110W flat field exposure from the first run of the TV3 SMS to the combined F110W flat formed from the average of all four runs. First, there are a couple dozen small features (10-20 pixels in size) scattered about the images that are due to particles located on the Channel Select Mechanism (CSM) mirror, which is in the beam and nearly in focus for IR channel images. These features have peak-to-peak residuals of up to ~10%.

Second, there is a large, diffuse “X” pattern with residuals of a few tenths of a percent in the ratio images. The “X” pattern is due to the fact that the obscurations of the optical stimulus, which supplied the external flat field illumination, are not in a conjugate plane to the cold mask in the WFC3 IR detector housing (R. Telfer, private communication). The stimulus structures and WFC3 cold mask structures, notably the spiders, thus move

relative to each other as a function of field position, causing variations in the illumination pattern.



Figure 4. The ratio of an individual F110W flat to the combined F110W flat.

The CSM particulate and stimulus “X” pattern features appear as residuals in the combined IR flats because the IR corrector mechanism optic was moved - as part of the WFC3 alignment procedures - between runs 2 and 3 of the IR flat field procedure. Motion of this optic moves the IR beam within the WFC3 optical train, which results in movement of these features in IR images. Taking ratios of images with the features in different positions naturally results in pairs of light and dark “ghost” residuals, as seen in Figure 4. Comparison of these “ghosts” with the combined flats shows that the effects of the CSM particles can be seen in the flats themselves, clearly producing small regions of reduced QE.

Because the “X” pattern is caused by the stimulus used for ground testing and will not appear in on-orbit WFC3 images, its presence in the IR flat field images will not be

appropriate for calibrating on-orbit data and will therefore need to be removed or dealt with in some other way, possibly through the use of “delta” flats, which can serve as a correction to the pixel-to-pixel flats. Similarly, the CSM particulate features will appear in on-orbit images, but their location in the field is likely to be shifted by a small amount relative to the ground-based flats due to adjustments of the IR channel optical alignment that will take place after WFC3 is installed in HST. Hence some type of correction to the existing flats, created from these ground-based data, will be needed in order to correctly calibrate on-orbit images.

CEI Verifications

These flat field data can be used to verify compliance with several WFC3 Contract End Item (CEI) specifications. The following sections address the specifications one at a time.

IR Detector Flat Field Uniformity

CEI specification 4.8.11.1 paragraph 1 requires that the IR detector be correctable to a uniform gain per pixel to $<2\%$ at all useable wavelengths and $<1\%$ between 1000-1800 nm, with a goal of $<0.5\%$ over that wavelength range. As was stated previously, the RMS residuals in a single flatfielded image from this set of data is $\sim 0.5\%$, which easily meets the requirements and is close to meeting the goal.

Paragraph 2 of this specification requires that no more than 5% of all pixels have response outside the range of 50-200% of the mean response, with a goal to have $<1\%$ of all pixels outside the range of 95-105%. The short-wavelength F098M flat field image, which has the largest variation in QE, has 0.2% of all pixels outside the 50-200% response range, but 19% outside of the 95-105% range. This detector therefore easily meets the requirement, but not the goal.

IR Detector Low Spatial Frequency Flat Field Structure

CEI specification 4.8.11.2 requires that large-scale flat field non-uniformities shall be correctable to $<2\%$. As was shown earlier, all large-scale QE features, such as the Wagon Wheel, are correctable to a few tenths of a percent, which easily meets this requirement. The only uncorrectable features are the Death Star and the unbonded pixels.

IR Detector Non-Functional Pixels

CEI specification 4.8.11.3 requires that no more than 2% (with a goal of 0.5%) of the pixels may be non-functional, where non-functional includes dead pixels, hot pixels (exceeding 100 times the median dark current), and pixels with uncorrected QEs less than 25% or more than 400% of the mean QE. Pixels that fall into the first and last categories amount to $\sim 0.27\%$, including the region of the Death Star. Hot pixels amount to $\sim 0.1\%$.

So the total amount of non-functional pixels is $\sim 0.37\%$, which meets both the requirement and the goal.

Summary

IR pixel-to-pixel flat field reference files have been created for the WFC3 IR4 flight detector using external flat field exposures obtained during TV3 ground testing. Flats for each of the 15 IR channel imaging filters have been created and ingested into CDBS for use in the WFC3 calibration pipeline. The reference flats have RMS noise levels of $\sim 0.2\%$. Both small- and large-scale regions of lower than normal QE in the detector are very stable and therefore calibrate well when the flats are applied to science images. The regions of lower than average QE are wavelength dependent, having lower response at shorter wavelengths.

There are certain artifacts in the delivered flat field reference files that will need to be corrected in order to properly calibrate on-orbit data. A large-scale, low-level “X” pattern appears in the flats, which comes from the optical stimulus used to obtain the ground flats. Furthermore, particulates on the CSM mirror appear as small regions of decreased QE in the flats. These will be present in on-orbit images, but are likely to appear at different locations once the on-orbit optical alignment has been performed. Movement of these features within the flats will need to be taken into account.

These data show that the IR4 detector meets all of the applicable flat field-related CEI requirements and several of the goals.

References

- Bushouse, H. 2008, WFC3 TIR 2008-03, “The WFC3/IR Flat-field Reference File Scripts,” in preparation.
- Kuntschner, H., Bushouse, H., Walsh, J. R., and Kümmel, M. 2008, WFC3 ISR 2008-16, “The TV3 ground calibrations of the WFC3 NIR grisms.”
- Martel, A. R., Baggett, S., Bushouse, H., and Sabbi, E. 2008, WFC3 TIR 2008-01, “The WFC3/UVIS Reference Files: 1. The Scripts.”
- Sabbi, E. 2008, WFC3 ISR 2008-46, “WFC3 UVIS Ground P-flats,” in preparation.

Appendix A: Exposure Catalog

Table 2 lists the individual TV3 IR13S01 exposures that were used to construct the IR pixel-to-pixel flat field images. Columns include the root name of the OPUS image file, ground-test image database ID number (“TVNUM”), filter name, number of IR samples in the exposure, and the WFC3 instrument electronics side (“MEB ID”) in use.

Table 2. Catalog of TV3 exposures used in the IR pixel-to-pixel flats.

OPUS File Name	TVNUM	Filter	Nsamp	MEB ID
ii131a01r_08074153434	51618	F098M	8	MEB1
ii130101r_08076234134	52177	F098M	8	MEB1
ii130101r_08096041532	56153	F098M	8	MEB2
ii130101r_08101043431	57160	F098M	8	MEB2
ii131a04r_08074154503	51620	F105W	4	MEB1
ii130104r_08076235153	52179	F105W	4	MEB1
ii130104r_08096042551	56155	F105W	4	MEB2
ii130104r_08101044450	57162	F105W	4	MEB2
ii131a06r_08074154503	51622	F110W	10	MEB1
ii130106r_08076235153	52181	F110W	9	MEB1
ii130106r_08096042551	56157	F110W	9	MEB2
ii130106r_08101044450	57164	F110W	9	MEB2
ii131a09r_08074155957	51624	F125W	10	MEB1
ii130109r_08077000638	52183	F125W	11	MEB1
ii130109r_08096044037	56159	F125W	11	MEB2
ii130109r_08101045936	57166	F125W	11	MEB2
ii131a0cr_08074161200	51626	F140W	8	MEB1
ii13010cr_08077001900	52185	F140W	8	MEB1
ii13010cr_08096045259	56161	F140W	8	MEB2
ii13010cr_08101051158	57168	F140W	8	MEB2
ii131a0fr_08074162046	51628	F160W	9	MEB1
ii13010fr_08077002826	52187	F160W	11	MEB1
ii13010fr_08096050225	56163	F160W	11	MEB2
ii13010fr_08101052124	57170	F160W	11	MEB2
ii131a0ir_08074163142	51630	F127M	9	MEB1
ii13010ir_08077004017	52189	F127M	7	MEB1
ii13010ir_08096051416	56165	F127M	7	MEB2
ii13010ir_08101053315	57172	F127M	7	MEB2
ii131a0lr_08074164246	51632	F139M	9	MEB1
ii13010lr_08077005044	52191	F139M	9	MEB1
ii13010lr_08096052443	56167	F139M	9	MEB2
ii13010lr_08101054342	57174	F139M	9	MEB2
ii131a0nr_08074164246	51634	F153M	6	MEB1
ii13010nr_08077005044	52193	F153M	8	MEB1
ii13010nr_08096052443	56169	F153M	8	MEB2
ii13010nr_08101054342	57176	F153M	8	MEB2
ii131a0qr_08074170105	51636	F126N	7	MEB1
ii13010qr_08077010854	52195	F126N	6	MEB1

WFC3 Instrument Science Report 2008-28

ii13010qr_08096054252	56171	F126N	6	MEB2
ii13010qr_08101060151	57178	F126N	6	MEB2
ii131a0sr_08074170105	51638	F128N	6	MEB1
ii13010sr_08077010854	52197	F128N	5	MEB1
ii13010sr_08096054252	56173	F128N	5	MEB2
ii13010sr_08101060151	57180	F128N	5	MEB2
ii131a0vr_08074171504	51640	F130N	5	MEB1
ii13010vr_08077012225	52199	F130N	5	MEB1
ii13010vr_08096055623	56175	F130N	5	MEB2
ii13010vr_08101061522	57182	F130N	5	MEB2
ii131a0xr_08074171504	51642	F132N	5	MEB1
ii13010xr_08077012225	52201	F132N	5	MEB1
ii13010xr_08096055623	56177	F132N	5	MEB2
ii13010xr_08101061522	57184	F132N	5	MEB2
ii131a10r_08074172813	51644	F164N	4	MEB1
ii130110r_08077013635	52203	F164N	6	MEB1
ii130110r_08096061034	56179	F164N	6	MEB2
ii130110r_08101062933	57186	F164N	6	MEB2
ii131a12r_08074172813	51646	F167N	4	MEB1
ii130112r_08077013635	52205	F167N	6	MEB1
ii130112r_08096061034	56181	F167N	6	MEB2
ii130112r_08101062933	57188	F167N	6	MEB2

Appendix B: Flat Field Image Atlas

Images of the IR channel pixel-to-pixels flats for each of the 15 filters are shown in Figures 5-19. The images are shown with a positive transform (lighter areas have higher flat-field values).

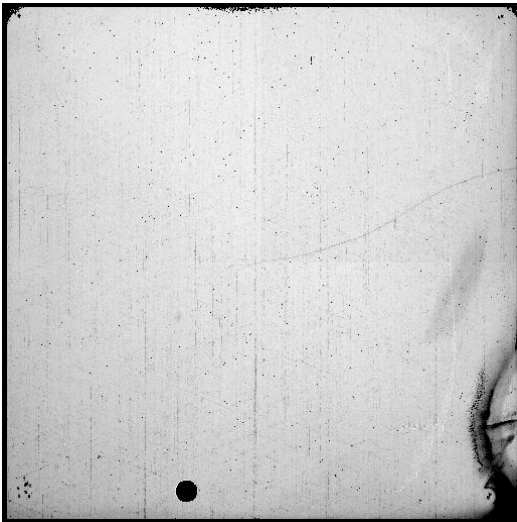


Figure 5. F098M flat field image.

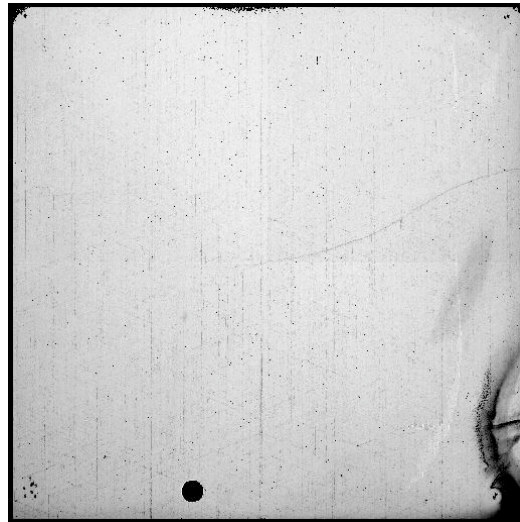


Figure 6. F105W flat field image.

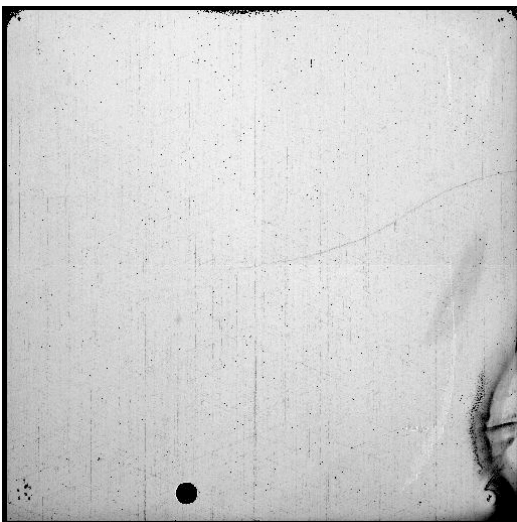


Figure 7. F110W flat field image.



Figure 8. F125W flat field image.

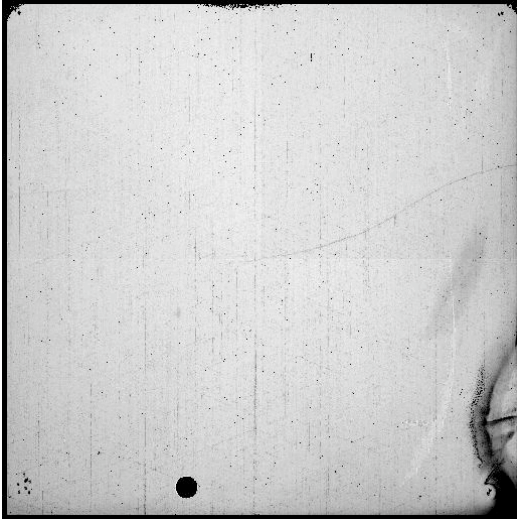


Figure 9. F126N flat field image.



Figure 10. F127M flat field image.

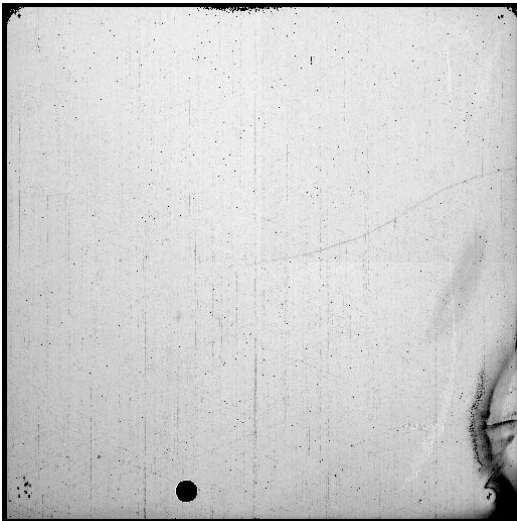


Figure 11. F128N flat field image.



Figure 12. F130N flat field image.

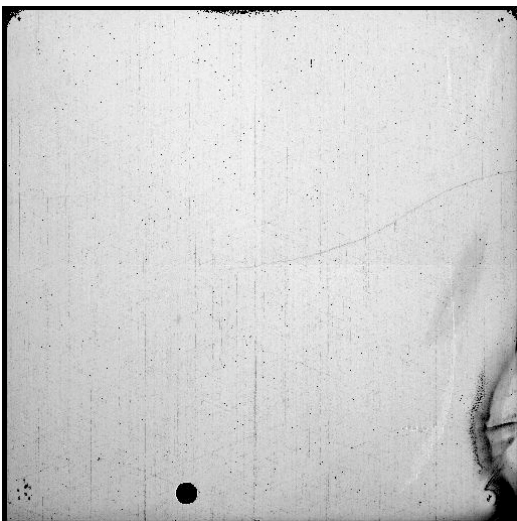




Figure 15. F140W flat field image.



Figure 16. F153M flat field image.



Figure 17. F160W flat field image.



Figure 18. F164N flat field image.



Figure 19. F167N flat field image.